Photoacoustic imaging based on MEMS mirror scanning

Lei Xi,[1] Jingjing Sun,[2] Yiping Zhu,[2] Lei Wu,[2] Huikai Xie,[2] and Huabei Jiang[1]

[1]*Department of Biomedical Engineering University of Florida*
Gainesville, Florida 32611, USA
[2]*Department of Electrical and Computer Engineering University of Florida*
Gainesville, Florida 32611, USA
**leix@ufl.edu*

Abstract: A microelectromechanical systems (MEMS)-based photoacoustic imaging system is reported for the first time. In this system, the MEMS-based light scanning subsystem and a ring-shaped polyvinylidene fluoride (PVDF) transducer are integrated into a miniaturized probe that is capable of three-dimensional (3D) photoacoustic imaging. It is demonstrated that the imaging system is able to image small objects embedded in phantom materials and in chicken and to in vivo visualize blood vessels under the skin of a human hand.

OCIS codes: (170.5120) Photoacoustic imaging; (170.0110) Imaging systems.

References and links

1. A. A. Oraevsky, S. L. Jacques, R. O. Esenaliev, and F. K. Tittel, "Laser based optoacoustic imaging in biological tissues," Proc. SPIE **2134A**, 122–128 (1994).
2. A. A. Oraevsky, and A. A. Karabutov, "Optoacoustic tomography," Chapter 34 in *Biomedical Photonics Handbook*, T. Vo-Dinh, ed. (CRC Press, Boca Raton, FL, 2003), Vol. PM125, pp. 34/1–34/34.
3. A. A. Oraevsky, A. A. Karabutov, and S. V. Solomatin, "Laser optoacoustic imaging of breast cancer *in vivo*," Proc. SPIE **4256**, 6–11 (2001).
4. S. Manohar, A. Kharine, J. C. G. van Hespen, W. Steenbergen, and T. G. van Leeuwen, "The Twente Photoacoustic Mammoscope: system overview and performance," Phys. Med. Biol. **50**(11), 2543–2557 (2005).
5. S. Manohar, A. Kharine, J. C. G. van Hespen, W. Steenbergen, and T. G. van Leeuwen, "Photoacoustic mammography laboratory prototype: imaging of breast tissue phantoms," J. Biomed. Opt. **9**(6), 1172–1181 (2004).
6. Q. Zhang, Z. Liu, P. R. Carney, Z. Yuan, H. Chen, S. N. Roper, and H. Jiang, "Non-invasive imaging of epileptic seizures *in vivo* using photoacoustic tomography," Phys. Med. Biol. **53**(7), 1921–1931 (2008).
7. Y. Sun, E. Sobel, and H. Jiang, "Quantitative three-dimensional photoacoustic tomography of the finger joints: an *in vivo* study," J. Biomed. Opt. **14**(6), 064002 (2009).
8. Y. Sun, and H. Jiang, "Quantitative three-dimensional photoacoustic tomography of the finger joints: phantom studies in a spherical scanning geometry," Phys. Med. Biol. **54**(18), 5457–5467 (2009).
9. J. A. Viator, G. Au, G. Paltauf, S. L. Jacques, S. A. Prahl, H. Ren, Z. Chen, and J. S. Nelson, "Clinical testing of a photoacoustic probe for port wine stain depth determination," Lasers Surg. Med. **30**(2), 141–148 (2002).
10. B. Yin, D. Xing, Y. Wang, Y. Zeng, Y. Tan, and Q. Chen, "Fast photoacoustic imaging system based on 320-element linear transducer array," Phys. Med. Biol. **49**(7), 1339–1346 (2004).
11. E. Z. Zhang, J. G. Laufer, R. B. Pedley, and P. C. Beard, "*In vivo* high-resolution 3D photoacoustic imaging of superficial vascular anatomy," Phys. Med. Biol. **54**(4), 1035–1046 (2009).
12. J. Sun, S. Guo, L. Wu, L. Liu, S.-W. Choe, B. S. Sorg, and H. Xie, "3D in vivo optical coherence tomography based on a low-voltage, large-scan-range 2D MEMS mirror," Opt. Express **18**(12), 12065–12075 (2010).
13. P. H. Tran, D. S. Mukai, M. Brenner, and Z. Chen, "In vivo endoscopic optical coherence tomography by use of a rotational microelectromechanical system probe," Opt. Lett. **29**(11), 1236–1238 (2004).
14. J. M. Zara, S. Yazdanfar, K. D. Rao, J. A. Izatt, and S. W. Smith, "Electrostatic micromachine scanning mirror for optical coherence tomography," Opt. Lett. **28**(8), 628–630 (2003).
15. A. D. Aguirre, P. R. Hertz, Y. Chen, J. G. Fujimoto, W. Piyawattanametha, L. Fan, and M. C. Wu, "Two-axis MEMS scanning catheter for ultrahigh resolution three-dimensional and en face Imaging," Opt. Express **15**(5), 2445–2453 (2007).
16. Z. Xie, S. Jiao, H. F. Zhang, and C. A. Puliafito, "Laser-scanning optical-resolution photoacoustic microscopy," Opt. Lett. **34**(12), 1771–1773 (2009).

#133714 - $15.00 USD Received 23 Aug 2010; revised 30 Sep 2010; accepted 29 Oct 2010; published 2 Nov 2010

17. L. Wu, and H. Xie, "A large vertical displacement electrothermal bimorph microactuator with very small lateral shift," Sens. Actuators A Phys. **145–146**, 371–379 (2008).

1. Introduction

Biomedical photoacoustic imaging is an emerging technology based on photoacoustic effect. It combines high optical contrast and high ultrasound resolution in a single imaging modality [1,2]. It has been thus far demonstrated that photoacoustic imaging has the potential to image breast cancer, skin disorder, brain vasculature, arthritis and seizure focus [3–11].

Photoacoustic imaging using miniaturized scanning systems/probes represents a new direction in this field. Such a miniaturized system allows for high resolution/high contrast photoacoustic imaging in applications such as endoscopic screening and image-guided surgery. One of the existing methods is based on mechanical scanning of a single transducer using geared micromotor, which can realize only two dimensional and side-view imaging without an external linear stage. Another one is to use galvanometer scanner with a larger size of mirror for scanning the laser beam which needs a relatively large space to assemble the probe. On the other hand, microelectromechanical systems (MEMS) mirrors can manipulate laser beams in free space, eliminating optical coupling non-uniformity and instability. Two-dimensional (2D) MEMS mirrors can also perform fast roster scanning [12–16].

In this paper, we report for the first time a 2D MEMS-based scanning system for 3D photoacoustic imaging. In this system, we use a 2D MEMS mirror based on thermal bimorph actuation mechanism to realize fast light scanning and a single element ring-shaped PVDF transducer to detect ultrasound signals. Three dimensional images of pencil lead(s) embedded in phantom materials and chicken legs and images of in vivo human blood vessels are successfully obtained using this MEMS-based photoacoustic system.

2. Photoacoustic imaging system

The schematic of the experimental setup is shown in Fig. 1(a), in which a MEMS mirror [see Fig. 1(d)], embedded in a small-diameter scanning probe [Fig. 1(b)], is used to perform laser beam scanning and an Nd:YAG 532 nm laser (NL 303HT from EKSPLA, Lithuania) is employed to generate pulses of 20 ns duration at 10 Hz. The laser beam via a reflection mirror is delivered into the scanning probe. A laser beam of 1×1 mm^2 in size is formed through an aperture and re-directed by a fixed mirror/prism to the scanning MEMS mirror [Fig. 1(d)]. The PVDF ultrasound transducer is attached to the end of the scanning probe [Fig. 1(b)]. The home-made PVDF ultrasound transducer is a ring-shaped one-element ultrasound detector. It was fabricated using a 110μm-thick Ag ink printed PVDF film (Measurement Specialties Inc.) as the sensing unit, flexible PCBs as positive and negative electrode connectors, and backing materials. The inner and outer diameters of the probe are 9.5mm and 11.5mm, respectively. The central frequency is 2.5 MHz. The photograph of the probe is shown in Fig. 1(c).

As shown in Fig. 1(d) and Fig. 1(e), the MEMS mirror (aperture size = 1×1 mm^2 and footprint size = 2×2 mm^2) has four electrothermal bimorph-based actuators made from a lateral-shift-free large-vertical-displacement (LSF-LVD) design [17]. After released, the actuators will curl up and elevate the mirror plate out of plane. When applying a voltage generated by two function generators to the MEMS mirror, each actuator can move up or down due to the Joule heating effect, resulting in a tilt to the mirror plate. 2D scanning (up to a rate of 500 Hz) can be realized by applying different voltages to the four actuators as shown in Fig. 1(e) (Media 1).

In the system, an output trigger signal is used to synchronize the data acquisition and function generators (AFG3022B, Tektronics). The ultrasound signal is amplified by a pre-amplifier with a gain of 17dB and further amplified by an amplifier with a controllable gain from 5dB to 20dB. The data acquisition sampling rate is 50MHz and a band-pass filter (Panametrics, Waltham, Massachusetts) from 1MHz to 5MHz is used to cut off the low

#133714 - $15.00 USD Received 23 Aug 2010; revised 30 Sep 2010; accepted 29 Oct 2010; published 2 Nov 2010

frequency and electromagnetic noises. In the experiments, ultrasound gel is applied between the probe and the sample to minimize ultrasound attenuation.

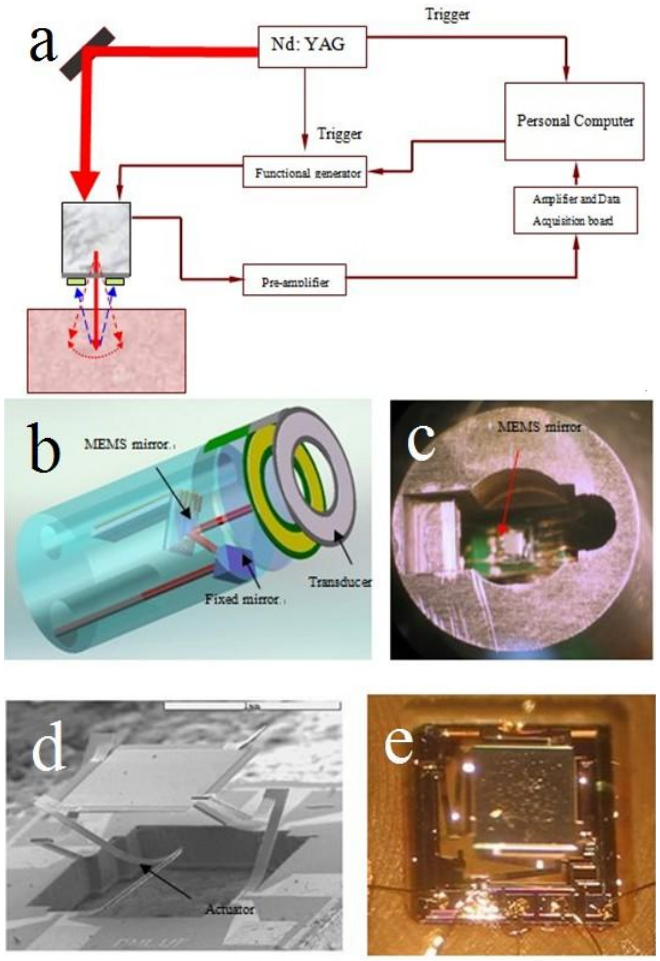

Fig. 1. (a) Schematic of our photoacoustic imaging system. 3D rendering (b) and photograph (c) of the scanning probe. (d), (e) Photograph of the MEMS mirror (Media 1).

3. Phantom/Chicken experiments

We demonstrate the ability of our imaging system through several phantom/chicken and in vivo experiments. In these experiments, the 532nm laser beam illuminated the sample surface over an area of 1 × 1 mm^2 at 15 mJ/cm^2 which is below the American National Standards Institute safety limit of 20 mJ/cm^2 . The four actuators driven by 0~4V differential ramp voltages were used for scanning an area of up to 9 × 9 mm^2 given a distance of 9 mm between MEMS mirror and image surface and an optical scan angle of ± 31° for the MEMS mirror .The scanning frequencies used were 100 and 2 mHz along X and Y directions to collect signals at 50 x 50 points. Due to the 10 Hz repetition rate of the laser, the scanning time is currently limited to 250s for the experiments performed.

In the phantom experiments, we placed the probe 6mm away from the phantom surface with ultrasound gel applied between the probe and the phantom. With a 90° directivity along the axial direction, the probe can cover an area of 24mm in diameter. As shown in Fig. 2(a), the pencil lead was embedded 1.2mm below the surface of a 50mm-diameter cylindrical solid phantom, consisting of Intralipid as the scatterer and India ink as the absorber. The phantom

#133714 - $15.00 USD Received 23 Aug 2010; revised 30 Sep 2010; accepted 29 Oct 2010; published 2 Nov 2010

had $\mu_a = 0.007mm^{-1}$ (absorption coefficient) and $\mu_s' = 1.0mm^{-1}$ (reduced scattering coefficient). Agar powder (2%) was used to solidify the Intralipid/ink suspensions. Figure 2(b) presents a typical A-line signal collected (blue line), along with its amplitude after the Hilbert transform (red line), while Fig. 2(c) shows the 2D image of the object. Using the criteria defined by the full-width-at-half maximum (FWHM) of multiple A-line signals, the size of the recovered object is estimated to be 0.72mm compared to the actual object size of 0.70mm. The signal-to-noise ratio (SNR) of the image signals was found to be 32dB which decreases with increased depth of the target. In this experiment, we placed the pencil lead at different depths and found that the imaging depth can be up to 2.5mm. We also found that the axial resolution is less than 0.5mm and that the lateral resolution is less than 0.7mm.

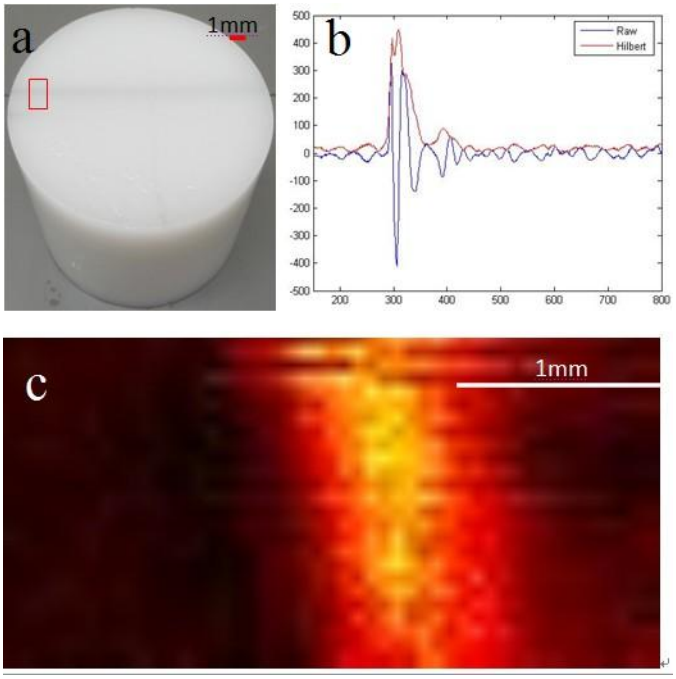

Fig. 2. (a) Photograph of a phantom containing a single object. (b) A typical raw signal (blue) and signal after the Hilbert transform (red). (c) The recovered 2D image.

Figure 3(a) and 3(b) gives the photograph and recovered image of another phantom where multiple targets were embedded at different positions/depths. From the image shown in Fig. 3(b), we see that the targets are all detected.

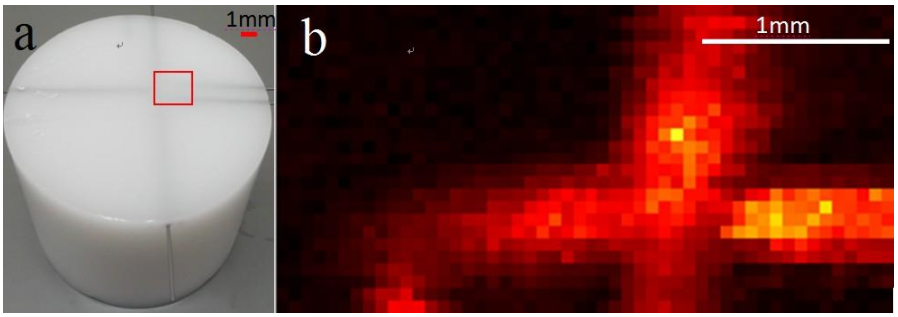

Fig. 3. Photograph of a phantom containing multiple objects (a) and the recovered 2D image (b).

#133714 - $15.00 USD Received 23 Aug 2010; revised 30 Sep 2010; accepted 29 Oct 2010; published 2 Nov 2010

The results given in Fig. 4 show the three dimensional imaging ability of our system. In this experiment, a pencil lead with a diameter of 0.7mm was embedded in one piece of chicken [Fig. 4(a)] at a depth of 1.5mm from the surface. The recovered 3D images are presented in Fig. 4(b)–4(d) (at coronal, sagittal- and cross-section views) and in Fig. 4(e) (3D rendering of the recovered image). Again, the object is accurately imaged in terms of its size, shape and location.

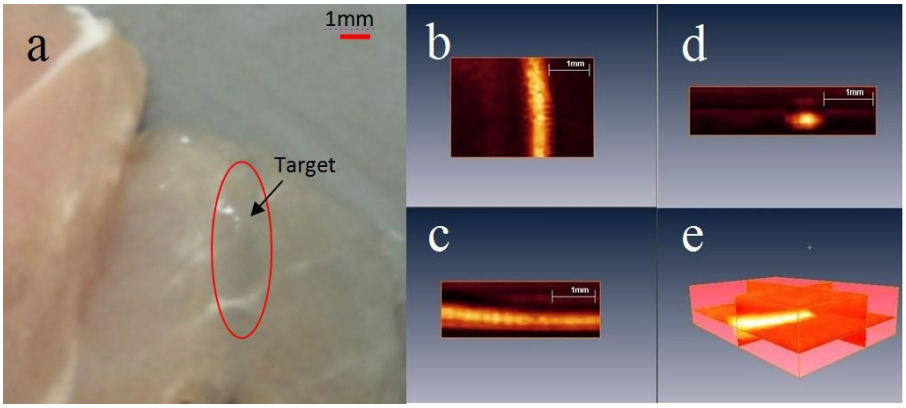

Fig. 4. (a) Photograph of the chicken with an embedded object. (b)-(d): coronal, sagittal and cross-section views of the recovered 3D image. (e): the 3D rendering of the recovered image.

4. In vivo imaging of blood vessels

Here we demonstrate the in vivo imaging ability of our MEMS-based photoacoustic imaging system for visualizing blood vessels in a human hand. The photograph of the hand and the barely visible blood vessels under the skin are shown in Fig. 5(a), while the recovered 3D image of the blood vessels is given in Fig. 5(b). We can see that the blood vessels are clearly imaged with correct shape and size for most part. We also note that some middle portions of the blood vessels [indicated by arrow in Fig. 5(b)] are notably distorted or missing. This is most likely attributed to the fact that these portions of the blood vessels are physically located deeper over other parts of the blood vessels of interest and that the sensitivity of the transducer responsible for this part of the imaging area is lower due to the limited directivity of the transducer used. It is noted that the shape of the vessels is not round likely due to the non-linear effect of the MEMS mirror. We are seeking ways to resolve this issue by using a proper calibration method.

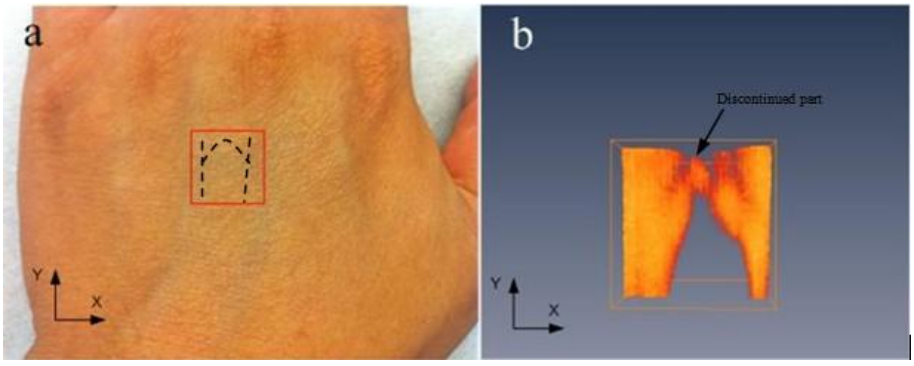

Fig. 5. (a) Photograph of the hand with highlighted imaging area. (b) 3D rendering of the recovered blood vessels.

#133714 - $15.00 USD Received 23 Aug 2010; revised 30 Sep 2010; accepted 29 Oct 2010; published 2 Nov 2010

5. Conclusions

In this paper, we have demonstrated a MEMS-based photoacoustic imaging system using both phantom and in vivo experiments. While promising, we realize some limitations associated with our current system. First, the imaging area of 9×9 mm^2 is relatively small limited by the voltages applicable to the current MEMS actuators. We are investigating to optimize the MEMS mirror design to increase the scan angle. Second, the scanning speed of the system is limited by the relatively low repetition frequency of the laser. We note that pulsed lasers with a repetition frequency of up to 200Hz are already available commercially, making real-time imaging possible in our next generation system. Third, the axial resolution can be increased by increasing the frequency of the transducer, by decreasing the thickness of the PVDF film to the range of 28-52μm, or by using more sensitive piezocomposite materials based transducer. Finally, the quick decay of optical fluence in turbid medium should be considered, and we plan to use optical fiber plus GRIN lens to achieve highly focused light beam for deeper penetration. The results obtained from this study are encouraging, and the probe diameter will be reduced to 5mm or smaller, which will allow us to develop a MEMS-based photoacoustic imaging system for image-guided surgery in future. For endoscopic applications, the probe diameter will be further reduced to 3mm or smaller.

#133714 - $15.00 USD Received 23 Aug 2010; revised 30 Sep 2010; accepted 29 Oct 2010; published 2 Nov 2010